The Astrophysical Journal Letters, 850:L19 (8pp), 2017 December 1 https://doi.org/10.3847/2041-8213/aa991c

Constraining the Maximum Mass of Neutron Stars from Multi-messenger Observations of GW170817

Ben Margalit and Brian D. Metzger
Department of Physics and Columbia Astrophysics Laboratory, Columbia University, New York, NY 10027, USA
btm2134@columbia.edu, bdm2129@columbia.edu
Received 2017 October 17; revised 2017 November 7; accepted 2017 November 7; published 2017 November 21

Abstract

We combine electromagnetic (EM) and gravitational-wave (GW) information on the binary neutron star (NS) merger GW170817 in order to constrain the radii $R_{\rm ns}$ and maximum mass $M_{\rm max}$ of NSs. GW170817 was followed by a range of EM counterparts, including a weak gamma-ray burst (GRB), kilonova (KN) emission from the radioactive decay of the merger ejecta, and X-ray/radio emission consistent with being the synchrotron afterglow of a more powerful off-axis jet. The type of compact remnant produced in the immediate merger aftermath, and its predicted EM signal, depend sensitively on the high-density NS equation of state (EOS). For a soft EOS that supports a low $M_{\rm max}$, the merger undergoes a prompt collapse accompanied by a small quantity of shock-heated or disk-wind ejecta, inconsistent with the large quantity $\gtrsim 10^{-2}\,M_\odot$ of lanthanide-free ejecta inferred from the KN. On the other hand, if $M_{\rm max}$ is sufficiently large, then the merger product is a rapidly rotating supramassive NS (SMNS), which must spin down before collapsing into a black hole. A fraction of the enormous rotational energy necessarily released by the SMNS during this process is transferred to the ejecta, either into the GRB jet (energy $E_{\rm GRB}$) or the KN ejecta (energy $E_{\rm ej}$), also inconsistent with observations. By combining the total binary mass of GW170817 inferred from the GW signal with conservative upper limits on $E_{\rm GRB}$ and $E_{\rm ej}$ from EM observations, we constrain the likelihood probability of a wide range of previously allowed EOSs. These two constraints delineate an allowed region of the $M_{\rm max}$–$R_{\rm ns}$ parameter space, which, once marginalized over NS radius, places an upper limit of $M_{\rm max} \lesssim 2.17\,M_\odot$ (90%), which is tighter or arguably less model-dependent than other current constraints.

Key words: equation of state – gravitational waves – stars: neutron

1. Introduction

On 2017 August 17, the Advanced Laser Interferometer Gravitational-wave Observatory (LIGO) and Virgo network of gravitational-wave (GW) observatories discovered the inspiral and coalescence of a binary neutron star (BNS) system (LIGO Scientific Collaboration & Virgo Collaboration 2017), dubbed GW170817. The measured binary chirp mass was $\mathcal{M}_{\rm c} = 1.118^{+0.004}_{-0.002}\,M_\odot$, with larger uncertainties on the mass of the individual neutron star (NS) components and total mass of $M_1 = 1.36$–$1.60\,M_\odot$, $M_2 = 1.17$–$1.36\,M_\odot$, and $M_{\rm tot} = M_1 + M_2 = 2.74^{+0.04}_{-0.01}\,M_\odot$, respectively. These masses are derived under the prior of low dimensionless NS spin ($\chi \lesssim 0.05$), characteristic of Galactic BNS systems.

The electromagnetic follow-up of GW170817 was summarized in LIGO Scientific Collaboration et al. (2017a). The *Fermi* and *INTEGRAL* satellites discovered a sub-luminous gamma-ray burst (GRB) with a sky position and temporal coincidence within $\lesssim$2 s of the inferred coalescence time of GW170817 (Goldstein et al. 2017; LIGO Scientific Collaboration et al. 2017b; Savchenko et al. 2017). Eleven hours later, an optical counterpart was discovered (Allam et al. 2017; Arcavi et al. 2017; Coulter et al. 2017; Lipunov et al. 2017; Yang et al. 2017; Tanvir et al. Levan 2017) with a luminosity, thermal spectrum, and rapid temporal decay consistent with those predicted for "kilonova" (KN) emission, powered by the radioactive decay of heavy elements synthesized in the merger ejecta (Li & Paczyński 1998; Metzger et al. 2010). The presence of both early-time visual ("blue") emission (Metzger et al. 2010), which transitioned to near-infrared ("red") emission (Barnes & Kasen 2013; Tanaka & Hotokezaka 2013) at late times, requires at least two distinct ejecta components consisting, respectively, of light and heavy *r*-process nuclei (e.g., Chornock et al. 2017; Cowperthwaite et al. 2017; Drout et al. 2017; Kasen et al. 2017; Kasliwal et al. 2017; Nicholl et al. 2017). Rising X-ray (Margutti et al. 2017; Troja et al. 2017) and radio (Alexander et al. 2017; Hallinan et al. 2017) emission was observed roughly two weeks after the merger, consistent with the delayed onset of the synchrotron afterglow of a more powerful relativistic GRB, with an emission that was initially relativistically beamed away from our line of sight (e.g., van Eerten & MacFadyen 2011).

The discovery of GW170817 implies a BNS rate of $\mathcal{R}_{\rm BNS} = 1540^{+3200}_{-1220}\,{\rm Gpc^{-3}\,yr^{-1}}$, corresponding to ≈6–120 BNS mergers per year once LIGO/Virgo reach design sensitivity (LIGO Scientific Collaboration & Virgo Collaboration 2017). This relatively high rate bodes well for the prospects of several scientific objectives requiring a large population of GW detections, such as "standard siren" measurements of the cosmic expansion history (Holz & Hughes 2005; Nissanke et al. 2010; LIGO Scientific Collaboration et al. 2017c) or as probes of the equation of state (EOS) of NSs (e.g., Read et al. 2009; Hinderer et al. 2010; Bauswein & Janka 2012).

Uncertainties in the EOS limit our ability to predict key properties of NSs, such as their radii and maximum stable mass (e.g., Özel & Freire 2016). Methods to measure NS radii from GWs include searching for tidal effects on the waveform during the final stages of the BNS inspiral (Damour & Nagar 2010; Hinderer et al. 2010; Damour et al. 2012; Del Pozzo et al. 2013; Read et al. 2013; Favata 2014; Agathos et al. 2015; Chatziioannou et al. 2015; Lackey & Wade 2015) and for quasi-periodic oscillations of the post-merger remnant (e.g., Bauswein & Janka 2012; Bauswein et al. 2012; Clark

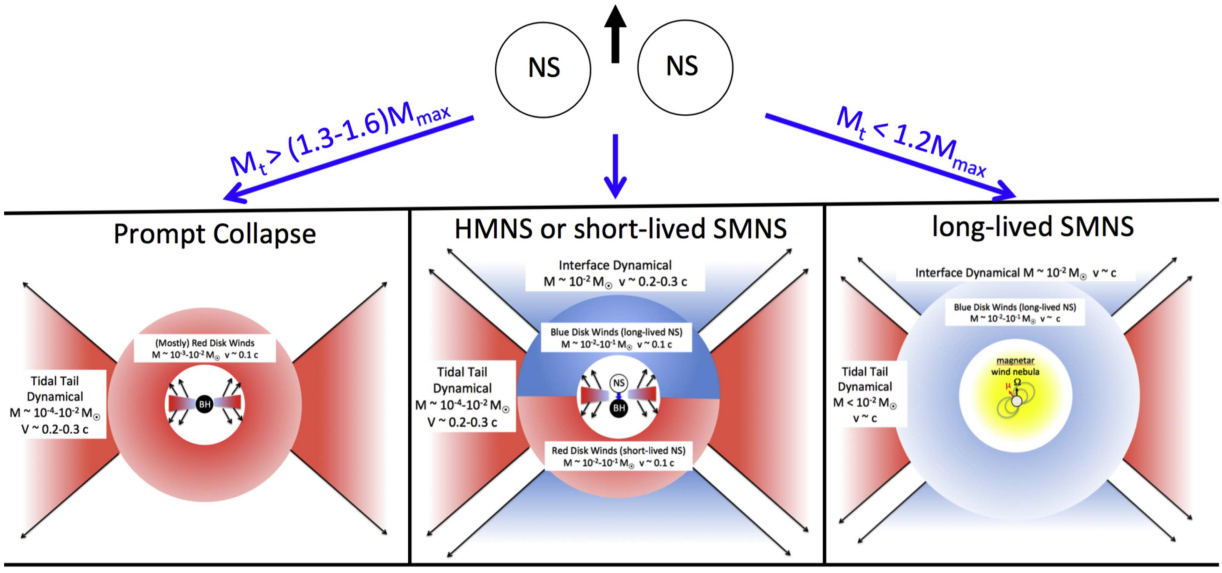

Figure 1. The strength of the red and blue KN signatures of a BNS merger depends upon the compact remnant that forms immediately after the merger; the latter, in turn, depends upon the total mass of the original binary or its remnant, $M_{\rm tot}$, relative to the maximum NS mass, $M_{\rm max}$. A massive binary ($M_{\rm tot} \gtrsim 1.3$–$1.6M_{\rm max}$) results in a prompt collapse to a BH; in such cases, the polar shock-heated ejecta is negligible and the accretion disk outflows are weakly irradiated by neutrinos, resulting in a primarily red KN powered by the tidal ejecta (left panel). By contrast, a very low-mass binary $M_{\rm tot} \lesssim 1.2M_{\rm max}$ creates a long-lived SMNS, which imparts its large rotational energy $\gtrsim 10^{52}$ erg to the surrounding ejecta, imparting relativistic expansion speeds to the KN ejecta or producing an abnormally powerful GRB jet (right panel). In the intermediate case, $1.2M_{\rm max} \lesssim M_{\rm tot} \lesssim 1.3$–$1.6M_{\rm max}$ a HMNS or short-lived SMNS forms, which produces both blue and red KN ejecta expanding at mildly relativistic velocities, consistent with observations of GW170817.

et al. 2014; Bauswein & Stergioulas 2015; Bauswein et al. 2016). Searches on timescales of tens of ms to $\lesssim$500 s post-merger revealed no evidence for such quasi-periodic oscillations in GW170817 (LIGO Scientific Collaboration & Virgo Collaboration 2017).

While the radii of NS are controlled by the properties of the EOS at approximately twice the nuclear saturation density, the maximum stable mass (Lattimer & Prakash 2001), $M_{\rm max}$ instead depends on the very high-density EOS (around eight times the saturation density; Özel & Psaltis 2009). Observations of two pulsars with gravitational masses of $1.93 \pm 0.07\ M_\odot$ (Demorest et al. 2010; Özel & Freire 2016) or $2.01 \pm 0.04\ M_\odot$ (Antoniadis et al. 2013) place the best current lower bounds. However, other than the relatively unconstraining limit set by causality, no firm theoretical or observational upper limits exist on $M_{\rm max}$. Indirect, assumption-dependent limits on $M_{\rm max}$ exist from observations of short GRBs (e.g., Lasky et al. 2014; Fryer et al. 2015; Lawrence et al. 2015; Piro et al. 2017) and by modeling the mass distribution of NSs (e.g., Antoniadis et al. 2016; Alsing et al. 2017).

Despite the large uncertainties on $M_{\rm max}$, it remains one of the most important properties affecting the outcome of a BNS merger and its subsequent electromagnetic (EM) signal (Figure 1). If the total binary mass $M_{\rm tot}$ exceeds a critical threshold of $M_{\rm th} \approx kM_{\rm max}$, then the merger product undergoes "prompt" dynamical-timescale collapse to a black hole (BH; e.g., Shibata 2005; Shibata & Taniguchi 2006; Baiotti et al. 2008; Hotokezaka et al. 2011), where the proportionality factor $k \approx 1.3-1.6$ is greater for smaller values of the NS "compactness", $C_{\rm max} = (GM_{\rm max}/c^2R_{1.6})$, where $R_{1.6}$ is the radius of a $1.6\,M_\odot$ NS (e.g., Bauswein et al. 2013). For slightly less-massive binaries with $M_{\rm tot} \lesssim M_{\rm th}$, the merger instead produces a hyper-massive neutron star (HMNS), which is supported from collapse by differential rotation (and, potentially, by thermal support). For lower values of $M_{\rm tot} \lesssim 1.2\,M_{\rm max}$, the merger instead produces a supramassive neutron star (SMNS), which remains stable even once its differential rotation is removed, as is expected to occur $\lesssim$10–100 ms following the merger (Baumgarte et al. 2000; Paschalidis et al. 2012; Kaplan et al. 2014). A SMNS can survive for several seconds, or potentially much longer, until its rigid body angular momentum is removed through comparatively slow processes, such as magnetic spin-down. Finally, for an extremely low binary mass, $M_{\rm tot} \lesssim M_{\rm max}$, the BNS merger produces an indefinitely stable NS remnant (e.g., Bucciantini et al. 2012; Giacomazzo & Perna 2013). Figure 2 shows the baryonic mass thresholds of these possible BNS merger outcomes (prompt collapse, HMNS, SMNS, stable) for an example EOS as vertical dashed lines.

The different types of merger outcomes are predicted to create qualitatively different electromagnetic (EM) signals (e.g., Bauswein et al. 2013; Metzger & Fernández 2014). In this Letter, we combine EM constraints on the type of remnant that formed in GW170817 with GW data on the binary mass in order to constrain the radii and maximum mass of NSs.

2. Constraints from EM Counterparts

This section reviews what constraints can be placed from EM observations on the energy imparted by a long-lived NS into the non-relativistic KN ejecta (Section 2.1) and into the relativistic ejecta of the GRB jet (Section 2.2). Then in Section 2.3 we describe the implications for the type of remnant formed.

2.1. Kilonova (Non-relativistic Ejecta)

Two sources of neutron-rich ejecta, capable of synthesizing *r*-process nuclei, accompany a BNS merger (Fernández & Metzger 2016). First, matter is ejected on the dynamical timescale, either by tidal forces (e.g., Ruffert et al. 1997; Rosswog et al. 1999; Radice et al. 2016) or by shock heating at the interface between the merging NSs (e.g., Oechslin

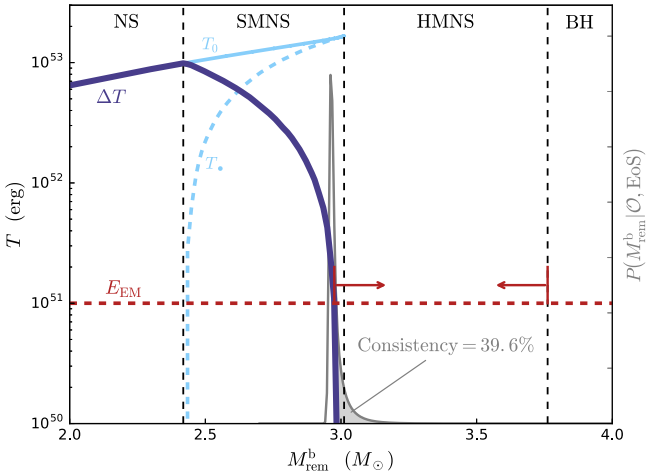

Figure 2. Maximum extractable rotational energy of the merger remnant $\Delta T = T_0 - T_*$ (Equation (1)) is shown as a dark-blue solid curve for a sample EOS. Vertical dashed curves demarcate the range of baryonic remnant masses $M^{\rm b}_{\rm rem}$ for which the immediate post-merger compact object is a stable NS, SMNS, HMNS, or a BH (prompt collapse). A horizontal red dashed curve shows the maximal energy transferred to the environment of the merger consistent with EM observations of GW170817 for the GRB and KN emission. The parameter space where $\Delta T \gg E_{\rm EM}$ is thus ruled out. The prompt-collapse scenario is also ruled out (see the text), such that $M^{\rm b}_{\rm rem}$ is constrained within an "allowed" region shown by red arrows. The gray curve shows the remnant mass probability distribution function (Equation (4)), and the consistency is the integral over this distribution within the allowed region (Equation (6); shaded gray area).

et al. 2007a; Bauswein et al. 2013; Hotokezaka et al. 2013). The tidal matter emerges in the binary equatorial plane and has a low electron fraction, $Y_e \lesssim 0.1$–0.2. Matter from the shocked interface expands into the polar direction and possesses a higher $Y_e \gtrsim 0.25$ (Wanajo et al. 2014; Sekiguchi et al. 2016).

Outflows from the accretion torus around the central compact object provide a second important source of ejecta (e.g., Metzger et al. 2008a; Siegel & Metzger 2017a, 2017b; Dessart et al. 2009; Fernández & Metzger 2013; Perego et al. 2014; Just et al. 2015). The disk outflows typically possess a broad distribution of $Y_e \sim 0.1$–0.5, with an average Y_e that increases with the lifetime of the HMNS/SMNS, due to neutrino irradiation of the ejecta by the NS (Metzger & Fernández 2014; Perego et al. 2014; Martin et al. 2015).

The KN following GW170817 showed evidence of two distinct emitting ejecta components (Cowperthwaite et al. 2017; Kasen et al. 2017; Tanaka et al. 2017). The early $\lesssim$2 day timescale "blue" emission phase requires an ejecta mass of $M_{\rm ej}^{\rm blue} \approx 1 \times 10^{-2}\,M_\odot$ of lanthanide-free ejecta ($Y_e \gtrsim 0.25$) with a mean velocity of $v_{\rm ej}^{\rm blue} \approx 0.2$–$0.3c$ (Nicholl et al. 2017). The comparatively "red" emission seen at later times requires $M_{\rm ej}^{\rm red} \approx 4$–$5 \times 10^{-2}\,M_\odot$ of lanthanide-rich ejecta ($Y_e \lesssim 0.25$) with $v_{\rm ej}^{\rm red} \approx 0.1$–$0.2c$ (Chornock et al. 2017). The total kinetic energy of the ejecta is therefore approximately $E_{\rm KN} \approx M_{\rm ej}^{\rm blue}(v_{\rm ej}^{\rm blue})^2/2 + M_{\rm ej}^{\rm red}(v_{\rm ej}^{\rm red})^2/2 \approx 1.0 \times 10^{51}$ erg.

2.2. Gamma-Ray Burst (Relativistic Ejecta)

The radiated gamma-ray energy from GW170817, and the kinetic energy of its afterglow if it originates from an on-axis GRB jet, were several orders of magnitude lower than those of cosmological short GRBs (Fong et al. 2017; Goldstein et al. 2017; LIGO Scientific Collaboration et al. 2017b). This could indicate that we are observing the GRB jet well outside of its core (e.g., Kathirgamaraju et al. 2017; Lazzati et al. 2017). The delayed rise of synchrotron X-ray and radio emission is consistent with the afterglow from a much more powerful relativistic jet pointed away from our line of sight (Alexander et al. 2017; Evans et al. 2017; Haggard et al. 2017; Hallinan et al. 2017; Troja et al. 2017; Margutti et al. 2017). However, for observing viewing angles relative to the binary axis inferred from the GW data and host galaxy, $\theta_{\rm obs} \approx 11^\circ - 33^\circ$ (LIGO Scientific Collaboration et al. 2017c), the inferred kinetic energy of an off-axis GRB jet is $E_{\rm GRB} \lesssim 10^{50}$ erg (e.g Alexander et al. 2017; Margutti et al. 2017), within the range of inferred properties of normal cosmological SGRB jets (Berger 2014).

The production of a GRB may indicate that a BH formed (e.g., Murguia-Berthier et al. 2014; Lawrence et al. 2015), in which case the GRB's delay of $\lesssim$2 s following the merger implicates a remnant that either underwent prompt collapse to a BH, or formed a short-lived HMNS or SMNS. It has been suggested that late-time X-ray emission observed after many short GRBs indicates the presence of a long-lived magnetar (e.g., Metzger et al. 2008b; Rowlinson et al. 2013), raising doubt about whether BH formation is a strict requirement for the production of a GRB. However, GW170817 showed no evidence for temporally extended high-energy emission (LIGO Scientific Collaboration et al. 2017b).

2.3. Constraints on the Merger Remnant in GW170817

The KN emission from GW170817 tightly constrains the type of compact remnant that formed in the merger event (Figure 1). Prompt collapse to a BH ($M_{\rm tot} \gtrsim M_{\rm th}$) is disfavored by the quantity of the blue KN ejecta. General relativistic numerical simulations show that mergers with prompt collapses eject only a small quantity $\lesssim 10^{-4}$–$10^{-3}\,M_\odot$ of matter from the merger interface (e.g., Hotokezaka et al. 2011), inconsistent with the inferred value $M_{\rm ej}^{\rm blue} \gtrsim 10^{-2}\,M_\odot$ for GW170817. The accretion disk outflows can also contribute; however, the wind ejecta with $Y_e \gtrsim 0.25$ is only a fraction of the initial torus, which is already small $\lesssim$0.01–0.02 $M_\odot$ for prompt collapse (Ruffert & Janka 1999; Shibata & Taniguchi 2006; Oechslin et al. 2007b). Furthermore, the predicted velocities of the disk winds $\sim$0.03–0.1c (e.g., Fernández & Metzger 2013; Just et al. 2015) are lower than the velocities $\gtrsim$0.2–0.3c inferred for the blue KN of GW170817 (e.g., Nicholl et al. 2017).

An HMNS remnant, due to its longer lifetime $\gtrsim$10 ms, produces a higher quantity of dynamical and disk-wind ejecta. The expansion rate $\sim$0.2–0.3c and ejecta mass of $M_{\rm ej}^{\rm blue} \approx 0.01$–$0.02\,M_\odot$ of the blue KN ejecta inferred for GW170817 are consistent with the properties of the high-Y_e shock-heated dynamical ejecta found by BNS merger simulations (e.g., Sekiguchi et al. 2016), provided that the radius of the NS is relatively small, $R_{\rm ns} \lesssim 11$ km (Nicholl et al. 2017). The higher quantity and lower velocity of the red KN emission are also broadly consistent with those expected from the outflows of a relatively massive accretion torus $\approx$0.1–0.2 $M_\odot$ (e.g., Siegel & Metzger 2017b) following the collapse of a relatively short-lived HMNS.

At the other extreme, a long-lived SMNS or indefinitely stable NS remnant is strongly disfavored by the moderate kinetic energy of the observed KN and GRB afterglow. Even

once its differential rotation has been removed, a SMNS possesses an enormous rotational energy, $T \approx 10^{53}$ erg, which is available to be deposited into the post-merger environment. Not all of this energy is "extractable" insofar as, even just prior to spinning down to the threshold for collapse, the NS remnant is still rotating quite rapidly. Margalit et al. (2015) showed that the collapse of an SMNS is unlikely to produce a centrifugally supported accretion disk outside of the innermost stable circular orbit, in which case all of the mass and angular momentum of the star are trapped in the BH.

The extractable rotational energy of a BNS merger remnant is more precisely defined as

$$\Delta T = T_0 - T_\bullet, \quad (1)$$

where T_0 is the energy available immediately after differential rotation has been removed, and $T_\bullet$ is the rotational energy at the point of gravitational collapse to a BH. We take T_0 equal to the rotational energy at the mass-shedding limit, a condition that approximates the state of the remnant immediately after differential rotation is removed. However, the constraints obtained hereafter would be similar if we had instead taken T_0 to equal the threshold value $T/|W| \approx 0.14$ for the growth of secular instabilities (e.g., Lai & Shapiro 1995). Figure 2 shows that ΔT rises sharply from zero at the HMNS–SMNS boundary to $\Delta T = T_0 \approx 10^{53}$ erg for stable remnants.

The most likely mechanism by which ΔT is removed, enabling the SMNS to collapse, is the extraction of angular momentum via a magnetized outflow or jet. MHD BNS merger simulations find that ultra-strong magnetic fields $\gtrsim 10^{15}$–10^{16} G are generated in the merger remnant (e.g., Kiuchi et al. 2014). An NS of radius $R_{\rm ns}$, rotation frequency $\Omega = 2\pi/P$, and spin period P loses energy to a magnetic wind at a rate (Spitkovsky 2006)

$$\dot{E}_{\rm mag} = \frac{\mu^2 \Omega^4}{c^3}(1 + \sin^2\chi), \quad (2)$$

where $B_{\rm d}$, $\mu = B_{\rm d} R_{\rm ns}^3$, and χ is the surface magnetic dipole field strength, dipole moment, and angle between the rotation and dipole axes, respectively. Taking $R_{\rm ns} = 12$ km and $\chi = 0$, the SMNS's available rotational energy is removed by magnetic torques on a timescale

$$\tau_{\rm sd} = \frac{\Delta T}{\dot{E}_{\rm mag}} \approx 24\ {\rm s}\left(\frac{\Delta T}{10^{52}\ {\rm erg}}\right)\left(\frac{B_{\rm d}}{10^{15}\ {\rm G}}\right)^{-2}\left(\frac{P}{0.8\ {\rm ms}}\right)^{4}. \quad (3)$$

If we demand that BH formation occur on a timescale of $\tau_{\rm sd} \lesssim 2$ s following the merger in order to explain the observed gamma-ray emission (Section 2.2), then this requires a SMNS remnant with $B_{\rm d} \gg 10^{15}$ G or $\Delta T \ll 10^{53}$ erg.

An SMNS can in principle also spin down through gravitational-wave emission, as may result from the quadrupolar moment of inertia induced by a strong interior magnetic field that is misaligned with the rotation axis (e.g., Stella et al. 2005; Dall'Osso et al. 2009, 2015). Figure 3 shows that GW spin-down dominates over magnetic spin-down (Equation (2)) only if the interior toroidal magnetic field exceeds the external poloidal one by a factor of $\gtrsim 100$. However, such a strong toroidal to poloidal field configuration would be unstable (Braithwaite 2009; Akgün et al. 2013; gray shaded region in Figure 3) and would furthermore imply a relatively long collapse time of $\tau_{\rm sd} \gtrsim 100$ s, potentially

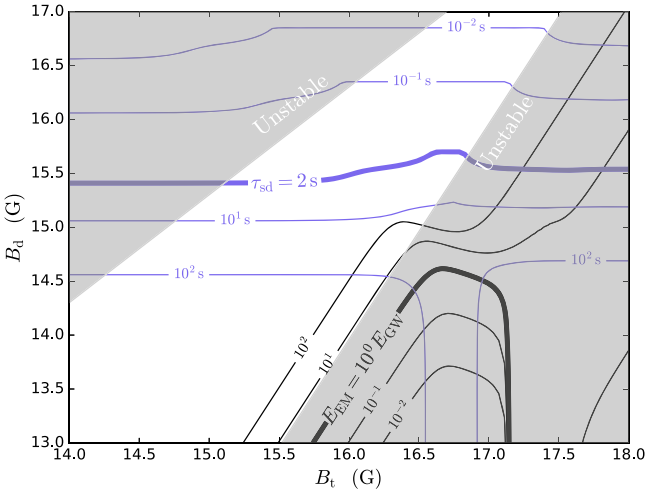

Figure 3. Parameter space of external dipole magnetic field $B_{\rm d}$, responsible for EM spin-down (Equation (2)), and internal toroidal field $B_{\rm t}$, which can deform the NS causing GW-driven spin-down. Contours show the spin-down timescale (blue) and ratio of EM-to-GW extracted spin-down energy (black) calculated by integrating equations for the spin frequency Ω and misalignment angle χ as a function of time (Cutler & Jones 2001; Dall'Osso et al. 2009). The region where GWs could dominate over EM emission falls below the thick black curve, but this region is: (a) susceptible to magnetic instabilities (gray shaded areas; Braithwaite 2009; Akgün et al. 2013), (b) implies long spin-down timescales $\gtrsim 100$ s at odds with the detection of a GRB only 2 s after the merger, and (c) would produce a strong GW signal.

incompatible with the gamma-ray burst emission observed on a timescale $\lesssim 2$ s (Section 2.2). It would also produce quasi-periodic GW emission, which is not observed in the GW170817 post-merger signal (albeit with only weakly constraining upper limits; LIGO Scientific Collaboration et al. 2017).

In summary, all signs point to GW170817 having produced an HMNS or very short-lived SMNS remnant. If the merger had instead produced a long-lived SMNS, then a large fraction of its available rotational energy $\gtrsim 10^{52}$ erg should have been deposited into the merger environment, either into a collimated relativistic jet or shared more equitably with the merger ejecta, on a timescale $\sim \tau_{\rm sd}$. Such a large energy input is incompatible with the GRB and KN observations of GW170817.

3. Constraints on NS Properties

The masses of the binary components inferred for GW170817, combined with evidence from the KN disfavoring a prompt collapse, places a lower limit on the maximum mass $M_{\rm max}$ of a (slowly rotating) NS. Likewise, upper limits on the rotational energy injected by a long-lived SMNS place an upper limit on $M_{\rm max}$.

In order to translate GW+EM inferences into constraints on the properties of NSs, we use the `RNS` code (Stergioulas & Friedman 1995) to construct general relativistic rotating hydrostationary NS models for a range of nuclear EOSs. We use the piecewise polytropic approximations to EOSs available in the literature provided in Read et al. 2009 (circles in Figure 4; summarized in Table 1), supplemented by EOSs constructed from the two-parameter piecewise polytropic parameterization of Margalit et al. (2015; triangles in Figure 4). Our simplified parameterization is limited in its ability to model micro-physically motivated EOS with high accuracy, yet it allows us to efficiently survey the EOS parameter space, and we leave it to future work to extend this

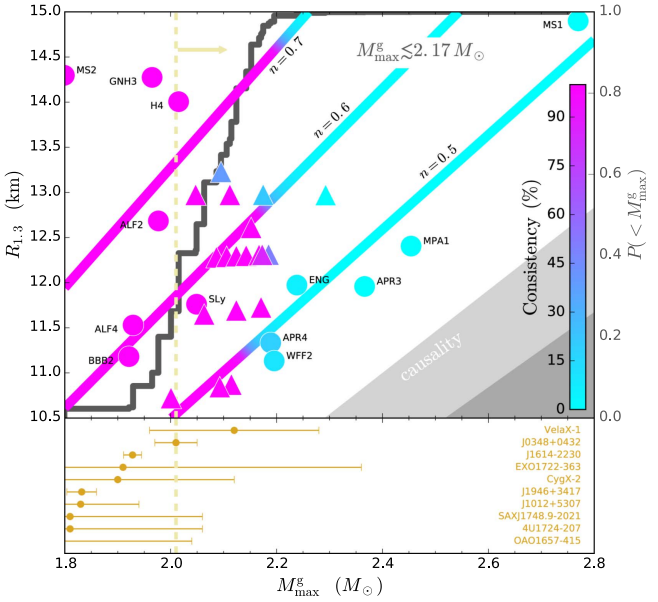

Figure 4. Constraints on properties of the NS EOS—radius of a 1.3 $M_\odot$ NS, $R_{1.3}$, and maximal non-rotating gravitational mass, $M^{\rm g}_{\rm max}$—based on joint GW-EM observations of GW170817. Different EOSs are represented as points, the color of which corresponds to the consistency of the given EOS with observational constraints. The similarly colored diagonal curves represent polytropic EOSs of index n, while the gray shaded regions to the bottom right are ruled out by the requirement of causality (see the text). Clearly, a low NS maximal mass is preferred due to constraints ruling out SMNS formation. The background gray curve shows the cumulative probability distribution function that the maximum mass $M^{\rm g}_{\rm max}$ is less than a given value (see the text), from which we find $M^{\rm g}_{\rm max} \lesssim 2.17\,M_\odot$ at 90% confidence. The bottom panel shows masses of observed Galactic NSs, from which a lower limit on $M^{\rm g}_{\rm max}$ can be placed (vertical dashed line).

Table 1
EOS Properties and Consistency with EM Observations

EOS	$M^{\rm g}_{\rm max}$ $(M_\odot)$	$R_{1.3}$ (km)	$M^{\rm g}_{\rm smns}$ $(M_\odot)$	$\Delta T_{\rm max}$ $(10^{53}$erg)	Consistency (%)
MS1	2.77	14.9	3.31	1.8	0.0
MPA1	2.45	12.4	2.97	1.8	0.0
APR3	2.37	12.0	2.84	1.7	0.2
ENG	2.24	12.0	2.67	1.4	5.2
WFF2	2.20	11.1	2.63	1.6	10.2
APR4	2.19	11.3	2.61	1.5	18.4
SLy	2.05	11.8	2.43	1.2	100.0
H4	2.02	14.0	2.38	0.8	100.0
ALF2	1.98	12.7	2.41	0.9	100.0
GNH3[a]	1.96	14.3	2.29	0.7	100.0
ALF4[a]	1.93	11.5	2.35	1.0	99.8
BBB2[a]	1.92	11.2	2.27	1.1	99.4
MS2[a]	1.80	14.3	2.10	0.6	99.9

Note. All EOSs are approximated as piecewise broken polytropes (Read et al. 2009).
[a] Ruled out by $2.01 \pm 0.04\,M_\odot$ mass of PSR J0348+0432 (Antoniadis et al. 2013).

first analysis with more flexible EOS parameterizations (e.g., Raithel et al. 2016). For each EOS, the uncertainty range of the GW170817-measured binary gravitational mass (LIGO Scientific Collaboration & Virgo Collaboration 2017) translates into a corresponding uncertainty range of baryonic mass, defined by the probability distribution

$$P(M^{\rm b}_{\rm rem}|\mathcal{O}, \mathrm{EoS}) = \int dM^{\rm b}_1 \int dM^{\rm b}_2 \;\; \delta(M^{\rm b}_1 + M^{\rm b}_2 - M_{\rm ej} - M^{\rm b}_{\rm rem}) \times P(g_{\rm EoS}(M^{\rm b}_1), g_{\rm EoS}(M^{\rm b}_2)|\mathcal{O}) |g'_{\rm EoS}(M^{\rm b}_1)||g'_{\rm EoS}(M^{\rm b}_2)|. \quad (4)$$

Here $P(M^{\rm g}_1, M^{\rm g}_2|\mathcal{O})$ is the posterior joint probability distribution function of NS gravitational masses inferred from the BNS waveform $\mathcal{O}$ (LIGO Scientific Collaboration & Virgo Collaboration 2017), $M_{\rm ej} = 2 \times 10^{-2}\,M_\odot$ is a conservative lower limit for the mass loss from the system as inferred from the KN ejecta, and the EOS enters in converting between gravitational and baryonic masses, $M^{\rm g} = g_{\rm EoS}(M^{\rm b})$. We approximate the posterior by changing variables to the chirp mass $\mathcal{M}_{\rm c}$ and mass-ratio $q = M^{\rm g}_1/M^{\rm g}_2$,

$$P(M^{\rm g}_1, M^{\rm g}_2|\mathcal{O}) = P(q, \mathcal{M}_{\rm c})\,\mathcal{M}_{\rm c}^{-1} q^{6/5}(1+q)^{-2/5}, \quad (5)$$

assuming independent asymmetric Gaussian distributions for both $P(\mathcal{M}_{\rm c})$ and $P(q)$, consistent with the median and 90% quoted confidence levels on $\mathcal{M}_{\rm c}$, $M^{\rm g}_1$, $M^{\rm g}_2$, and $M^{\rm g}_{\rm tot}$. Specifically, we assume $P(q, \mathcal{M}_{\rm c}) \propto \exp[-(\mathcal{M}_{\rm c} - \mu_{\mathcal{M}}, \pm)^2/2\sigma^2_{\mathcal{M}} - (q-\mu_q)^2/2\sigma^2_q]$ for $q \leqslant 1$ and $P = 0$ otherwise, with $\mu_q = 1$, $\sigma_q \simeq 0.164$, $\mu_{\mathcal{M}} \simeq 1.188\,M_\odot$ and where $\sigma_{\mathcal{M},\pm} \simeq 2.63 \times 10^{-3}\,M_\odot$ $(2.07 \times 10^{-3}\,M_\odot)$ for $\mathcal{M}_{\rm c} \geqslant \mu_{\mathcal{M}}$ $(\mathcal{M}_{\rm c} < \mu_{\mathcal{M}})$, respectively.

For each EOS, we then compare the inferred remnant mass to the "allowed" range between the maximum mass to avoid prompt collapse (using the relation $M_{\rm th}(R_{1.6}, M_{\rm max})$ of Bauswein et al. 2013), to the minimum baryonic mass, which results in an SMNS with an extractable energy ΔT (Equation (1)) less than the upper limits on the kinetic energy of the KN and GRB emission $E_{\rm EM} = E_{\rm KN} + E_{\rm GRB} \lesssim 10^{51}$ erg. Integrating the probability distribution of the remnant mass within this allowed range yields the "consistency" of the given EOS with the GW170817 observations,

$$\text{Consistency} = \int_S P(M^{\rm b}_{\rm rem}|\mathcal{O}, \mathrm{EoS})\, dM^{\rm b}_{\rm rem}, \quad (6)$$

where S is the domain in which both $\Delta T(M^{\rm b}_{\rm rem}) \leqslant E_{\rm EM}$ and $M^{\rm b}_{\rm rem} \leqslant M_{\rm th}$.

One example of this analysis is illustrated in Figure 2. Clearly, $E_{\rm EM}$ is so much smaller than $\Delta T_{\rm max}$ that the extractable energy curve intersects $E_{\rm EM}$ at the very precipice of the SMNS–HMNS transition. We also find for all of the EOSs that we have examined that $M^{\rm b}_{\rm smns} \approx 1.18 M^{\rm b}_{\rm max}$ largely irrespective of compactness, consistent with previous findings (e.g., Lasota et al. 1996). These two facts allow for the formulation of an approximate analytic criterion on the maximal non-rotating NS mass consistent with GW170817,

$$M^{\rm b}_{\rm max} \lesssim M^{\rm b}_{\rm rem}/\xi, \quad (7)$$

where $\xi \simeq 1.16$–1.21 and the EOS is only necessary in translating baryonic to gravitational masses.

In addition to several key properties of each EOS, Table 1 provides the probability that each EOS is consistent with constraints from GW170817. For instance, the very hard MS1, MPA1, and ENG EOS are disfavored, with consistencies of 0.0%, 0.0% and 5.2%, respectively. However, the softer EOSs with $M^{\rm g}_{\rm max} \lesssim 2.1$–$2.2\,M_\odot$ show much higher consistencies.

Figure 4 shows where each of our EOSs lie in this $M_{\rm max}$–$R_{1.3}$ parameter space, with the strength of the symbol representing the probability of its consistency with GW170817. Additionally shown are consistency values for polytropic EOSs of the form $P \propto \rho^{1+1/n}$ with indices $n = 0.5, 0.6, 0.7$. These define diagonal curves in the $M^{\rm g}_{\rm max}$–$R_{1.3}$ plane parameterized by the pressure normalization of the polytrope. Regions of large compactness are ruled out by the requirement of causality, $R_{\rm max} \geqslant 2.82 G M^{\rm g}_{\rm max}/c^2$ (dark shaded region; Koranda et al. 1997), which is conservative as $R_{1.3}$ is generally larger than the radius of a maximum mass NS, $R_{\rm max}$. A tighter estimate of $R_{1.3} \geqslant 3.1 G M^{\rm g}_{\rm max}/c^2$ is therefore also shown (light shaded region). The background gray curve shows the cumulative probability distribution function that the maximum mass $M_{\rm max}$ is less than a given value. This was calculated by marginalizing over the $R_{1.3}$ axis and treating the consistency values as points in a probability distribution function. We weight the EOS with $M^{\rm g}_{\rm max}$ below 2.01 $M_\odot$ by a Gaussian prior accounting for consistency with the maximum measured pulsar mass of $2.01 \pm 0.04\,M_\odot$ (Antoniadis et al. 2013). Thus, we find $M^{\rm g}_{\rm max} \lesssim 2.17\,M_\odot$ at 90% confidence.

4. Discussion

Several works have explored the potentially exotic EM signals of BNS mergers in cases when a long-lived SMNS or stable neutron star remnant is formed (Metzger et al. 2008b; Bucciantini et al. 2012; Yu et al. 2013; Metzger & Bower 2014; Metzger & Piro 2014; Gao et al. 2016; Siegel & Ciolfi 2016a, 2016b). However, one of the biggest lessons from GW170817 was the well-behaved nature of its EM emission, under the simplest case of a relatively short-lived HMNS remnant (Shibata & Taniguchi 2006), with an off-axis afterglow (van Eerten & MacFadyen 2011) and KN emission (Metzger et al. 2010) closely resembling "vanilla" theoretical predictions.

Here we have made explicit the argument that the BNS merger GW170817 formed a HMNS. In combination with the GW-measured binary mass, this inferred outcome places upper and lower limits on the maximum NS mass. The lower limit on $M_{\rm max}$ is not constraining compared to those from well-measured pulsar masses, though tighter constraints would be possible by the future detection of similar fast-expanding blue KN ejecta (indicating HMNS formation) from a future BNS merger with a similar observing inclination but a higher binary mass than GW170817. The lack of a luminous blue KN following the short GRB050509b (Bloom et al. 2006; Metzger et al. 2010; Fong et al. 2017) may implicate a high-mass binary and prompt collapse for this event.[1]

On the other hand, our upper limits on $M_{\rm max} \lesssim 2.17\,M_\odot$ (90% confidence limit; Figure 4) are more constraining than the previous weak upper limits from causality, and less model-dependent than other methods (e.g., Lasky et al. 2014; Fryer et al. 2015; Lawrence et al. 2015; Gao et al. 2016; Alsing et al. 2017). A low value of $M_{\rm max}$ has also been suggested based on Galactic NS radius measurements (Özel et al. 2016; Özel & Freire 2016) and would be consistent with the relatively small NS radius $\lesssim$11 km inferred from modeling the blue KN (Cowperthwaite et al. 2017; Nicholl et al. 2017). Furthermore, the lack of measurable tidal effects in the inspiral of GW170817 similarly imply a small NS radius and thus a low $M_{\rm max}$ (LIGO Scientific Collaboration & Virgo Collaboration 2017). Upper limits on $M_{\rm max}$ will be improved by the future discovery of EM emission from a merger with a lower total mass than GW170817. Conversely, the detection of a substantially brighter afterglow or faster evolving KN emission could instead point to the formation of a long-lived SMNS or stable remnant. The NS masses measured for GW170817 are broadly consistent with being drawn from Galactic NS population, which is well-fit by a Gaussian of mean $\mu = 1.32\,M_\odot$ and standard deviation $\sigma = 0.11\,M_\odot$ (Kiziltan et al. 2013); this hints that the HMNS formation inferred in GW170817 is likely a common—if not the most frequent—outcome of a BNS merger.

A simple analytic estimate of our result can be obtained from Equation (7), using the approximation $M_{\rm b} = M_{\rm g} + 0.075 M_{\rm g}^2$ for the relation between baryonic and gravitational masses (Timmes et al. 1996). From this relation, the total baryonic binary mass is constrained, $M^{\rm b}_{\rm rem} \lesssim M^{\rm b}_{\rm tot} \lesssim 3.06\,M_\odot$. A typical value of $\xi \approx 1.18$ then implies that

$$M^{\rm g}_{\rm max} \lesssim \frac{\sqrt{1 + 0.3 M^{\rm b}_{\rm rem}/\xi} - 1}{0.15} \lesssim 2.2\,M_\odot, \quad (8)$$

in agreement with our more elaborately calculated result. We stress that the calculation above is intended only as an approximate analytic estimate, and that neither do we use the Timmes et al. (1996) relation nor do we assume a universal value for ξ in our complete analysis (Section 3).

Our approach differs in several respects from similar works constraining $M_{\rm max}$ (e.g., Lawrence et al. 2015; Fryer et al. 2015). These works generally assume (a) that the creation of a GRB implies that a BH formed, and (b) that BH formation necessarily implies either prompt collapse or an HMNS post-merger remnant. The central engine and emission mechanisms of GRBs are still widely debated in the literature, and the validity of the "GRB = BH" assumption remains unclear. Baryon-pollution by neutrino-driven winds launched off a long-lived NS remnant may hinder ultra-relativistic jets (Murguia-Berthier et al. 2014); however, the Lorentz factors of short GRB jets and GRB 170817A in particular are poorly constrained, and there remains room for the possibility that short GRBs may be powered by strongly magnetized rapidly rotating NSs. NS GRB engines have also been suggested on grounds of the "extended" X-ray emission observed after some short GRBs (e.g., Metzger et al. 2008b; Rowlinson et al. 2013), emission that is difficult to interpret within the BH engine model. Furthermore, the peculiar properties of GRB 170817A, accompanying GW170817, although broadly consistent with a normal GRB viewed off-axis (e.g., Margutti et al. 2017), may also point at a difference between this event and cosmological short GRBs (e.g., Gottlieb et al. 2017), necessitating further caution in the GRB modeling and interpretation. Even if a BH did form as a prerequisite to the GRB in this event (i.e., within $\sim$2 s post-merger), there is nothing a priori preventing this from occurring through the spin-down-induced collapse of an SMNS merger remnant, negating assumption (b) above. Here we have circumvented both assumptions and GRB engine modeling altogether by instead relying on a simple energetic consideration—that an SMNS merger remnant would inevitably release an enormous amount of rotational energy into the surrounding KN ejecta and circumstellar medium. Therefore, only merger remnants with an extractable rotational energy $\lesssim 10^{51}$ erg are

[1] A prompt collapse might also be consistent with the low measured gamma-ray fluence of GRB050509b, because the mass of the remnant accretion torus responsible for powering the GRB jet would also be lower for a prompt collapse than if a HMNS had formed.

consistent with the energetics inferred from EM observations of GW170817.

Several uncertainties affect our conclusions. Our upper limits on $M_{\rm max}$ implicitly assume that this is the most important parameter controlling the HMNS–SMNS boundary, and that the suite of EOSs that we have taken are sufficiently "representative" in the requisite sense. We cannot obviously exclude the possibility that an alternative EOS could be found with a large $M_{\rm max}$ that would still be consistent with our observational constraints.

Another uncertainty affecting our conclusions is the possibility that in counting the KN and GRB components of the ejecta, we are somehow "missing" substantial additional energy imparted by a putative SMNS remnant to the environment; however, any such hidden ejecta should be at least mildly relativistic and thus tightly constrained by radio synchrotron emission on timescales of months to years following the merger (Metzger & Bower 2014). Yet another uncertainty is the possibility that a SMNS did form, but most of its rotational energy was lost to GW radiation instead of being transferred to the merger ejecta. Though unlikely, we found this would only be possible for remnant lifetimes of $\sim$100 s (Figure 3). Searches in the GW170817 waveform have revealed no evidence for such signals, although the detectors' decreasing sensitivity at high frequencies currently limits these constraints (LIGO Scientific Collaboration et al. 2017).

Finally, our analysis neglects the effects of thermal pressure on the stability of the SMNS (Kaplan et al. 2014), which can be important on timescales of hundreds of milliseconds to seconds post-merger (depending also on the effects of neutrino-driven convection; Roberts et al. 2012). Thermal pressure in the outer layers of the star generally acts to reduce the maximum mass of the SMNS remnant by up to $\lesssim$8% (mainly by reducing the angular velocity at the mass-shedding limit), which would act to weaken our constraints on $M_{\rm max}$. Future numerical work exploring the transition from the HMNS to SMNS phase, which includes the effects of neutrino cooling and convection self-consistently, is required to better understand how this would quantitatively affect our conclusions.

B.M. and B.D.M. are supported in part by NASA through the ATP program, grant numbers NNX16AB30G and NNX17AK43G. The statistical analysis in this work would have greatly benefited from open access to the best-fit posterior parameter distributions obtained by LIGO Scientific Collaboration & Virgo Collaboration (2017).

ORCID iDs

Ben Margalit https://orcid.org/0000-0001-8405-2649

References

Agathos, M., Meidam, J., Del Pozzo, W., et al. 2015, PhRvD, 92, 023012
Akgün, T., Reisenegger, A., Mastrano, A., & Marchant, P. 2013, MNRAS, 433, 2445
Alexander, K. D., Berger, E., Fong, W., et al. 2017, ApJL, 848, L21
Allam, S., Annis, J., Berger, E., et al. 2017, GCN, 21530
Alsing, J., Silva, H. O., & Berti, E. 2017, arXiv:1709.07889
Antoniadis, J., Freire, P. C. C., Wex, N., et al. 2013, Sci, 340, 448
Antoniadis, J., Tauris, T. M., Ozel, F., et al. 2016, arXiv:1605.01665
Arcavi, I., Hosseinzadeh, G., Howell, D. A., et al. 2017, Natur, 551, 64
Baiotti, L., Giacomazzo, B., & Rezzolla, L. 2008, PhRvD, 78, 084033
Barnes, J., & Kasen, D. 2013, ApJ, 775, 18
Baumgarte, T. W., Shapiro, S. L., & Shibata, M. 2000, ApJL, 528, L29
Bauswein, A., Baumgarte, T. W., & Janka, H.-T. 2013, PhRvL, 111, 131101
Bauswein, A., & Janka, H.-T. 2012, PhRvL, 108, 011101
Bauswein, A., Janka, H.-T., Hebeler, K., & Schwenk, A. 2012, PhRvD, 86, 063001
Bauswein, A., & Stergioulas, N. 2015, PhRvD, 91, 124056
Bauswein, A., Stergioulas, N., & Janka, H.-T. 2016, EPJA, 52, 56
Berger, E. 2014, ARA&A, 52, 43
Bloom, J. S., Prochaska, J. X., Pooley, D., et al. 2006, ApJ, 638, 354
Braithwaite, J. 2009, MNRAS, 397, 763
Bucciantini, N., Metzger, B. D., Thompson, T. A., & Quataert, E. 2012, MNRAS, 419, 1537
Chatziioannou, K., Yagi, K., Klein, A., Cornish, N., & Yunes, N. 2015, PhRvD, 92, 104008
Chornock, R., Berger, E., Kasen, D., et al. 2017, ApJL, 848, L19
Clark, J., Bauswein, A., Cadonati, L., et al. 2014, PhRvD, 90, 062004
Coulter, D. A., Foley, R. J., Kilpatrick, C. D., et al. 2017, Sci, https://doi.org/10.1126/science.aap9811
Cowperthwaite, P. S., Berger, E., Villar, V. A., et al. 2017, ApJL, 848, L17
Cutler, C., & Jones, D. I. 2001, PhRvD, 63, 024002
Dall'Osso, S., Giacomazzo, B., Perna, R., & Stella, L. 2015, ApJ, 798, 25
Dall'Osso, S., Shore, S. N., & Stella, L. 2009, MNRAS, 398, 1869
Damour, T., & Nagar, A. 2010, PhRvD, 81, 084016
Damour, T., Nagar, A., & Villain, L. 2012, PhRvD, 85, 123007
Del Pozzo, W., Li, T. G. F., Agathos, M., Van Den Broeck, C., & Vitale, S. 2013, PhRvL, 111, 071101
Demorest, P. B., Pennucci, T., Ransom, S. M., Roberts, M. S. E., & Hessels, J. W. T. 2010, Natur, 467, 1081
Dessart, L., Ott, C. D., Burrows, A., Rosswog, S., & Livne, E. 2009, ApJ, 690, 1681
Drout, M. R., Piro, A. L., Shappee, B. J., et al. 2017, Sci, https://doi.org/10.1126/science.aaq0049
Evans, P. A., Cenko, S. B., Kennea, J. A., et al. 2017, Sci, https://doi.org/10.1126/science.aap9580
Favata, M. 2014, PhRvL, 112, 101101
Fernández, R., & Metzger, B. D. 2013, MNRAS, 435, 502
Fernández, R., & Metzger, B. D. 2016, Annu. Rev. Nucl. Part. Sci, 66, 23
Fong, W., Berger, E., Blanchard, P. K., et al. 2017, ApJL, 848, L23
Fryer, C. L., Belczynski, K., Ramirez-Ruiz, E., et al. 2015, ApJ, 812, 24
Gao, H., Zhang, B., & Lü, H.-J. 2016, PhRvD, 93, 044065
Giacomazzo, B., & Perna, R. 2013, ApJL, 771, L26
Goldstein, A., Veres, P., Burns, E., et al. 2017, ApJL, 848, L14
Gottlieb, O., Nakar, E., Piran, T., & Hotokezaka, K. 2017, arXiv:1710.05896
Haggard, D., Nynka, M., Ruan, J. J., et al. 2017, ApJL, 848, L25
Hallinan, G., Corsi, A., Mooley, K. P., et al. 2017, Sci, https://doi.org/10.1126/science.aap9855
Hinderer, T., Lackey, B. D., Lang, R. N., & Read, J. S. 2010, PhRvD, 81, 123016
Holz, D. E., & Hughes, S. A. 2005, ApJ, 629, 15
Hotokezaka, K., Kiuchi, K., Kyutoku, K., et al. 2013, PhRvD, 87, 024001
Hotokezaka, K., Kyutoku, K., Okawa, H., Shibata, M., & Kiuchi, K. 2011, PhRvD, 83, 124008
Just, O., Bauswein, A., Pulpillo, R. A., Goriely, S., & Janka, H.-T. 2015, MNRAS, 448, 541
Kaplan, J. D., Ott, C. D., O'Connor, E. P., et al. 2014, ApJ, 790, 19
Kasen, D., Metzger, B., Barnes, J., Quataert, E., & Ramirez-Ruiz, E. 2017, Natur, 551, 80
Kasliwal, M. M., Nakar, E., Singer, L. P., et al. 2017, Sci, https://doi.org/10.1126/science.aap9455
Kathirgamaraju, A., Barniol Duran, R., & Giannios, D. 2017, arXiv:1708.07488
Kiuchi, K., Kyutoku, K., Sekiguchi, Y., Shibata, M., & Wada, T. 2014, PhRvD, 90, 041502
Kiziltan, B., Kottas, A., De Yoreo, M., & Thorsett, S. E. 2013, ApJ, 778, 66
Koranda, S., Stergioulas, N., & Friedman, J. L. 1997, ApJ, 488, 799
Lackey, B. D., & Wade, L. 2015, PhRvD, 91, 043002
Lai, D., & Shapiro, S. L. 1995, ApJ, 442, 259
Lasky, P. D., Haskell, B., Ravi, V., Howell, E. J., & Coward, D. M. 2014, PhRvD, 89, 047302
Lasota, J.-P., Haensel, P., & Abramowicz, M. A. 1996, ApJ, 456, 300
Lattimer, J. M., & Prakash, M. 2001, ApJ, 550, 426
Lawrence, S., Tervala, J. G., Bedaque, P. F., & Miller, M. C. 2015, ApJ, 808, 186
Lazzati, D., Deich, A., Morsony, B. J., & Workman, J. C. 2017, MNRAS, 471, 1652
Li, L.-X., & Paczyński, B. 1998, ApJL, 507, L59

LIGO Scientific Collaboration & Virgo Collaboration 2017, PhRvL, 119, 161101
LIGO Scientific Collaboration & Virgo Collaboration, et al. 2017a, ApJL, 848, L12
LIGO Scientific Collaboration & Virgo Collaboration, et al. 2017b, ApJL, 848, L13
LIGO Scientific Collaboration & Virgo Collaboration, et al. 2017c, Natur, 551, 85, (http://adsabs.harvard.edu/cgi-bin/bib_query?arXiv:1710.05835)
Lipunov, V., Gorbovskoy, E., Kornilov, V. G., et al. 2017, GCN, 21546
Margalit, B., Metzger, B. D., & Beloborodov, A. M. 2015, PhRvL, 115, 171101
Margutti, R., Berger, E., Fong, W., et al. 2017, ApJL, 848, L20
Martin, D., Perego, A., Arcones, A., et al. 2015, ApJ, 813, 2
Metzger, B. D., & Bower, G. C. 2014, MNRAS, 437, 1821
Metzger, B. D., & Fernández, R. 2014, MNRAS, 441, 3444
Metzger, B. D., Martínez-Pinedo, G., Darbha, S., et al. 2010, MNRAS, 406, 2650
Metzger, B. D., & Piro, A. L. 2014, MNRAS, 439, 3916
Metzger, B. D., Piro, A. L., & Quataert, E. 2008a, MNRAS, 390, 781
Metzger, B. D., Quataert, E., & Thompson, T. A. 2008b, MNRAS, 385, 1455
Murguia-Berthier, A., Montes, G., Ramirez-Ruiz, E., De Colle, F., & Lee, W. H. 2014, ApJL, 788, L8
Nicholl, M., Berger, E., Kasen, D., et al. 2017, ApJL, 848, L18
Nissanke, S., Holz, D. E., Hughes, S. A., Dalal, N., & Sievers, J. L. 2010, ApJ, 725, 496
Oechslin, R., Janka, H.-T., & Marek, A. 2007a, A&A, 467, 395
Oechslin, R., Janka, H.-T., & Marek, A. 2007b, A&A, 467, 395
Özel, F., & Freire, P. 2016, ARA&A, 54, 401
Özel, F., & Psaltis, D. 2009, PhRvD, 80, 103003
Özel, F., Psaltis, D., Güver, T., et al. 2016, ApJ, 820, 28
Paschalidis, V., Etienne, Z. B., & Shapiro, S. L. 2012, PhRvD, 86, 064032
Perego, A., Rosswog, S., Cabezón, R. M., et al. 2014, MNRAS, 443, 3134
Piro, A. L., Giacomazzo, B., & Perna, R. 2017, ApJL, 844, L19
Radice, D., Galeazzi, F., Lippuner, J., et al. 2016, MNRAS, 460, 3255
Raithel, C. A., Özel, F., & Psaltis, D. 2016, ApJ, 831, 44
Read, J. S., Baiotti, L., Creighton, J. D. E., et al. 2013, PhRvD, 88, 044042
Read, J. S., Lackey, B. D., Owen, B. J., & Friedman, J. L. 2009, PhRvD, 79, 124032
Roberts, L. F., Shen, G., Cirigliano, V., et al. 2012, PhRvL, 108, 061103
Rosswog, S., Liebendörfer, M., Thielemann, F.-K., et al. 1999, A&A, 341, 499
Rowlinson, A., O'Brien, P. T., Metzger, B. D., Tanvir, N. R., & Levan, A. J. 2013, MNRAS, 430, 1061
Ruffert, M., & Janka, H.-T. 1999, A&A, 344, 573
Ruffert, M., Janka, H.-T., Takahashi, K., & Schaefer, G. 1997, A&A, 319, 122
Savchenko, V., Ferrigno, C., Kuulkers, E., et al. 2017, ApJL, 848, L15
Sekiguchi, Y., Kiuchi, K., Kyutoku, K., Shibata, M., & Taniguchi, K. 2016, PhRvD, 93, 124046
Shibata, M. 2005, PhRvL, 94, 201101
Shibata, M., & Taniguchi, K. 2006, PhRvD, 73, 064027
Siegel, D. M., & Ciolfi, R. 2016a, ApJ, 819, 14
Siegel, D. M., & Ciolfi, R. 2016b, ApJ, 819, 15
Siegel, D. M., & Metzger, B. D. 2017a, arXiv:1711.00868
Siegel, D. M., & Metzger, B. D. 2017b, arXiv:1705.05473
Spitkovsky, A. 2006, ApJL, 648, L51
Stella, L., Dall'Osso, S., Israel, G. L., & Vecchio, A. 2005, ApJL, 634, L165
Stergioulas, N., & Friedman, J. L. 1995, ApJ, 444, 306
Tanaka, M., & Hotokezaka, K. 2013, ApJ, 775, 113
Tanaka, M., Utsumi, Y., Mazzali, P. A., et al. 2017, arXiv:1710.05850
Tanvir, N. R., Levan, A. J., González-Fernández, C., et al. 2017, ApJL, 848, L27
The LIGO Scientific Collaboration, the Virgo Collaboration, Abbott, B. P., et al. 2017, arXiv:1710.09320
Timmes, F. X., Woosley, S. E., & Weaver, T. A. 1996, ApJ, 457, 834
Troja, E., Piro, L., van Eerten, H., et al. 2017, Natur, 551, 71
van Eerten, H. J., & MacFadyen, A. I. 2011, ApJL, 733, L37
Wanajo, S., Sekiguchi, Y., Nishimura, N., et al. 2014, ApJL, 789, L39
Yang, S., Valenti, S., Sand, D., et al. 2017, GCN, 21531
Yu, Y.-W., Zhang, B., & Gao, H. 2013, ApJL, 776, L40